

## THE AGES OF TYPE IA SUPERNOVA PROGENITORS

TIMOTHY D. BRANDT<sup>1</sup>, RITA TOJEIRO<sup>2</sup>, ÉRIC AUBOURG<sup>3,4,1</sup>, ALAN HEAVENS<sup>5</sup>, RAUL JIMENEZ<sup>6</sup>, AND MICHAEL A. STRAUSS<sup>1</sup>  
*Draft version July 29, 2010*

### ABSTRACT

Using light curves and host galaxy spectra of 101 Type Ia supernovae (SNe Ia) with redshift  $z \lesssim 0.3$  from the SDSS Supernova Survey (SDSS-SN), we derive the SN Ia rate as a function of progenitor age (the delay time distribution, or DTD). We use the VESPA stellar population synthesis algorithm to analyze the SDSS spectra of all galaxies in the field searched by SDSS-SN, giving us a reference sample of 77,000 galaxies for our SN Ia hosts. Our method does not assume any a priori shape for the DTD and therefore is minimally parametric. We present the DTD in physical units for high stretch (luminous, slow declining) and low stretch (subluminous, fast declining) supernovae in three progenitor age bins. We find strong evidence of two progenitor channels: one that produces high stretch SNe Ia  $\lesssim 400$  Myr after the birth of the progenitor system, and one that produces low stretch SNe Ia with a delay  $\gtrsim 2.4$  Gyr. We find that each channel contributes roughly half of the Type Ia rate in our reference sample. We also construct the average spectra of high stretch and low stretch SN Ia host galaxies, and find that the difference of these spectra looks like a main sequence B star with nebular emission lines indicative of star formation. This supports our finding that there are two populations of SNe Ia, and indicates that the progenitors of high stretch SNe are at the least associated with very recent star formation in the last few tens of Myr. Our results provide valuable constraints for models of Type Ia progenitors and may help improve the calibration of SNe Ia as standard candles.

*Subject headings:* Cosmology: Distance Scale, Galaxies: Stellar Content, Stars: Supernovae: General

### 1. INTRODUCTION

Type Ia supernovae (SNe Ia) are thought to be the products of a thermonuclear explosion of a white dwarf reaching the Chandrasekhar mass - the mass limit allowed by the supporting electron degeneracy pressure. This requires the white dwarf to accrete mass from a binary companion, though the nature of this companion and the timescale of the accretion are hotly debated. The *single degenerate* model proposes the companion to be a main sequence or giant star with mass transfer by Roche lobe overflow, while the *double degenerate* scenario proposes that the companion is also a white dwarf and the two objects merge. While the connection between these two scenarios and the delay time from progenitor birth to SN Ia explosion is unclear, knowledge of this delay would constrain the initial masses of SN Ia progenitors.

Interest in SNe Ia has greatly increased since their use as standardized candles led the discovery of the accelerated expansion of the Universe (Riess et al. 1998; Perlmutter et al. 1999). The latest generation of SN Ia surveys, including SNLS (Astier et al. 2006), ESSENCE (Wood-Vasey et al. 2007), and SDSS-SN (Kessler et al. 2009), however, are limited by the possibility of system-

atic uncertainties in their calibration of SN Ia luminosities. This has sparked great interest in any physical properties that could alter the peak luminosity/light curve width relation (Phillips 1993) used to calibrate SNe Ia. In particular, it has highlighted our incomplete knowledge of SN Ia progenitor systems.

Due to their low luminosities, SN Ia progenitors have never been directly observed. Constraints on their nature and rates of explosion must therefore come from studies of SN Ia environments, and a variety of techniques have been used to carry out such studies. Sullivan et al. (2006), Mannucci et al. (2006), and others use host galaxy photometry and Gallagher et al. (2005) use spectra to derive stellar populations and metallicities, and correlate these luminosity-weighted average values against SN Ia rates and properties. Sullivan et al. and Mannucci et al. see higher SN Ia rates in star-forming galaxies, while Gallagher et al. find that spirals host more luminous SNe. To derive constraints on the ages of the progenitor systems, Neill et al. (2006) and Gal-Yam & Maoz (2004) compare the evolution of the supernova rate with the evolution of the cosmic star formation rate. Because this rate changes slowly with redshift in the local universe, the method places only weak constraints on the progenitor ages. Cooper et al. (2009) have used host galaxy clustering as a proxy for the metallicities of SN Ia environments and found a significant correlation with supernova rate or luminosity. Badenes et al. (2009) have measured the *local* stellar populations for four historical SNe Ia in the Large Magellanic Cloud, finding that three of the supernovae live in regions with little star formation over the last several Gyr.

Over the past decade and a half, analyses of SN Ia environments (including several papers cited above) have produced evidence that there are at least two dis-

<sup>1</sup> Department of Astrophysical Sciences, Peyton Hall, Princeton University, Princeton, NJ 08544, USA

<sup>2</sup> Institute of Cosmology and Gravitation, University of Portsmouth, Dennis Sciama Building, Burnaby Road, Portsmouth, PO1 3FX

<sup>3</sup> Astroparticule et Cosmologie APC, UMR 7164, Université Paris Diderot, 10 rue Alice Domon et Léonie Duquet, 75205 Paris cedex 13, France

<sup>4</sup> CEA, Irfu, SPP, Centre de Saclay, 91191 Gif sur Yvette cedex, France

<sup>5</sup> SUPA, Institute for Astronomy, University of Edinburgh, Royal Observatory, Blackford Hill, Edinburgh EH9-3HJ, UK

<sup>6</sup> ICREA & Institute for Sciences of the Cosmos (ICCUB), University of Barcelona, Barcelona 08028, Spain

tinct populations of SNe Ia: blue, star-forming galaxies have higher supernova rates and host more luminous, slower-declining supernovae than do red, passive galaxies (Hamuy et al. 1996; Howell 2001; van den Bergh et al. 2005; Mannucci et al. 2005, but see Schawinski 2009). More recently, this conclusion has been confirmed in large, local SN Ia samples by Hicken et al. (2009) and Maoz et al. (2010) and in a higher redshift sample by Sullivan et al. (2010). The observation of at least two populations has led to the so-called  $A + B$  model (Scannapieco & Bildsten 2005), in which the supernova rate is modeled as the sum of a term proportional to total stellar mass (the delayed component) and a term proportional to recent star formation (the prompt component):

$$SNR = AM_* + BM_* \dot{M}_*. \quad (1)$$

Values of  $A$  and  $B$  have been determined by Sullivan et al. (2006), Neill et al. (2006), Mannucci et al. (2005) and others, with significant scatter between the groups due to different SN Ia samples, methods for deriving  $A$  and  $B$ , definitions of stellar masses and proxies for the star formation rates. Aubourg et al. (2008) used host galaxy spectra and found that the supernova rate per unit mass for young stars is  $\sim 500$  times higher than for old stellar populations, a factor of  $\sim 5$  higher than earlier results. They also found evidence that the time scale of the prompt component is  $\lesssim 180$  Myr.

Unfortunately, the  $A + B$  model provides only weak constraints on the ages associated with the prompt and delayed components. Because of the strong dependence of stellar evolution timescales on initial mass, more precise ages can powerfully constrain the main-sequence masses of the progenitors. This will require a better approximation to the full delay-time distribution (DTD), the explosion rate as a function of progenitor age. The DTD,  $\epsilon(t)$ , has units of number of supernovae per unit stellar mass per year, and relates a galaxy’s supernova rate to its star formation rate  $\psi(t)$ :

$$SNR(t) = \int_0^t \epsilon(t-t')\psi(t') dt'. \quad (2)$$

Thus,  $\epsilon(t)$  represents the probability per year that a unit of stellar mass will produce a Type Ia supernova a time  $t$  after its formation. The DTD sets the rates and timescales of SN Ia production that must be matched by progenitor models.

There have been several attempts to parametrize and measure the DTD. Pritchett et al. (2008) assume a continuous, power-law DTD ( $\epsilon(t) \propto t^{-p}$ ) and find that the SNLS survey constrains  $p$  to lie in the range  $0.3 \leq p \leq 0.7$ . Roughly speaking, this is required for consistency with measurements of  $A$  and  $B$  from, e.g., Sullivan et al. (2006). Using a theoretical argument to calculate the rate of white dwarf formation per unit stellar mass, they find that a single-degenerate model can yield a power law DTD of this form only if the fraction of white dwarfs which explode as SNe Ia is independent of progenitor mass. Because less massive progenitors should produce less massive remnants, Pritchett et al. conclude that there must be another, possibly double degenerate, route to SNe Ia. Totani et al. (2008) constrain the DTD in old stellar populations by selecting SN candidates in passive galaxies from the Subaru/XMM-Newton Deep Sur-

vey (SXDS, Furusawa et al. 2008). Combining these high redshift observations with the local observed SN Ia rate in ellipticals, they find  $\epsilon(t) \propto t^{-1}$  in the range  $0.1 < t < 10$  Gyr. Totani et al. argue that a DTD of this form supports a double-degenerate origin for delayed SNe Ia.

In this paper, we aim to provide better constraints on the DTD and to determine whether luminous SNe Ia (with temporally “stretched” light curves) and less luminous events have different progenitors from one another. Any attempt to measure the DTD relies on the intrinsic range of galaxy properties, and in particular, the differences between supernova hosts and non-hosts. It is therefore essential to have a supernova sample with a well-understood selection function and a well-defined control group of galaxies monitored for SNe. Otherwise, differences between hosts and non-hosts may be attributed to biases or survey systematics rather than to supernova rates. Nearby surveys often comprise SNe discovered by many different techniques, making it difficult to define or build a control sample. High redshift searches are often blind (i.e. sensitive to SNe in all galaxies in the field), but lack spectra of the field galaxies.

The Sloan Digital Sky Survey Supernova Survey (SDSS-SN, Frieman et al. 2008; Sako et al. 2008) satisfies both criteria. It is the only controlled, blind, difference imaging supernova search at low redshift, with most supernovae in the range  $0.05 \lesssim z \lesssim 0.35$ . SDSS (York et al. 2000) also has a large spectroscopic catalog of galaxies, of which about 83,000 lie in the stripe of sky monitored for supernovae. SDSS-SN is therefore the ideal survey with which to perform a statistical comparison of the spectroscopic properties of hosts and non-hosts.

For our study we select 101 SNe Ia from the SDSS-SN sample with acceptable light curves and SDSS host galaxy spectra. We then use VErSatile SPectral Analysis (Tojeiro et al. 2007) - VESPA - to derive star formation histories for all galaxies in the control sample. Given any assumed delay time distribution, these star formation histories allow us to simulate a population of hosts. We then use the spectra themselves to compare these mock hosts to the observed SN Ia host galaxies. We compute likelihoods for a large number of assumed delay time distributions, thereby constraining the DTD.

We have organized this paper as follows: in Section 2 we describe our datasets; in Sections 3 and 4 we describe our methodology; in Section 5 we present our results and we finally discuss and conclude in Section 6.

## 2. DATA: SDSS-SN

The SDSS Supernova Survey (SDSS-SN) was carried out along “Stripe 82” (York et al. 2000), a region of sky 2.5 degrees wide centered on the Celestial Equator, stretching from 20.7 hours to 3.9 hours ( $-50^\circ$  -  $+59^\circ$ ) Right Ascension for a total area of  $270 \text{ deg}^2$ . It was observed up to 80 times with the SDSS imaging camera (Gunn et al. 1998); supernova candidates were identified by difference imaging, and followed up with spectroscopy on other telescopes, and photometry from the SDSS telescope (Gunn et al. 2006) and other telescopes as well.

SDSS-SN is described in detail in Frieman et al. (2008) and Sako et al. (2008). Operating for three months of the year from 2005 to 2007, SDSS-SN has identified over 400

spectroscopically confirmed SNe Ia in the redshift range  $0.05 \lesssim z \lesssim 0.35$ , of which 146 from the 2005 season have *ugriz* light curves published in Holtzman et al. (2008). Preliminary data for the remainder were kindly provided to us by the SDSS supernova team. We have selected definitive and probable SNe Ia this catalog of preliminary photometry using the types reported through the Central Bureau for Astronomical Telegrams<sup>7</sup>. We have further excluded two objects listed as peculiar SNe Ia, 2005hk and 2007qd.

The preliminary photometric data lack errorbars, which we have estimated using the observed correlation between errors and magnitudes in each band in the published 2005 data (Holtzman et al. 2008). Because our final analysis only uses the light curves to divide our sample into two broad subsamples, our results are insensitive to the details of these error estimates. We have also checked the reliability of the preliminary flux measurements using objects from the 2005 season for which final data are also available. The differences between preliminary and final published fluxes are approximately Cauchy distributed, with a mean offset from zero of  $\sim 0.5 \mu\text{Jy}$  and a full width at half maximum of  $\sim 2.5 \mu\text{Jy}$ . These are much fainter than a typical SDSS supernova peak magnitude of  $\lesssim 20$ , or a peak flux of  $\gtrsim 40 \mu\text{Jy}$ .

The SDSS carried out spectroscopy of galaxies on Stripe 82, using the standard selection algorithms used throughout the SDSS survey. These include the Main Galaxy selection described in Strauss et al. (2002), consisting of all galaxies with Petrosian (1976) *r*-band magnitudes brighter than 17.77 and with a median redshift of order 0.13, and the Luminous Red Galaxy (LRG) sample of Eisenstein et al. (2001), which selects the most luminous red ellipticals to  $z \sim 0.55$ . Because of the limited imaging carried out by SDSS in the Fall months, however, additional spectroscopy was carried out on Stripe 82 using a variety of algorithms that went beyond the main spectroscopic sample (Adelman-McCarthy et al. 2006), including a sample designed to calibrate photometric redshifts, a sample of low-luminosity galaxies, an extension of the LRG sample to fainter and bluer objects, and a sample flux-limited in the *u*-band. In all, there are about 83,000 unique galaxies on Stripe 82 with spectroscopic data, of which only 23,000 were selected using the main survey algorithms. We have further excluded all galaxies with bad redshifts and, because we are interested in differences only in the *stellar* populations between SN Ia hosts and non-hosts, galaxies flagged as AGNs or QSOs by the SDSS pipeline. This leaves about 77,000 unique galaxies from the Seventh Data Release of SDSS (Abazajian et al. 2009), of which 22,000 are in the Main Galaxy Sample.

We have matched the SDSS-SN sample with this spectroscopic sample, yielding a total of 133 SNe with host spectra in SDSS. The light curves of these supernovae range in quality, but 101 are sufficiently good to measure parameters such as the peak flux and decline rate (see §3.2 and Figure 1 for examples). The 77,000 unique galaxies in Stripe 82 were not uniformly selected, and do not represent a flux-limited sample. However, our subsample of 101 SN hosts was selected from these 77,000 galaxies based solely on the occurrence of a detectable

SN Ia. These 101 SNe with SDSS hosts form the sample used in the rest of our analysis.

### 3. METHODOLOGY: INITIAL DATA ANALYSIS

To measure the delay time distribution, we need to be able to derive star formation histories for galaxies from their SDSS spectra. Because of the strong association of luminous (high stretch) SNe Ia with recent star formation seen by Sullivan et al. (2006) and others, we also investigate the dependence of the delay time distribution on supernova stretch. We begin by describing how we derive the star formation history and stretch from host galaxy spectrum and SN light curve, respectively. We then discuss the division of SNe Ia into a high stretch and a low stretch subgroup, and finally introduce the average spectra of Type Ia supernova hosts.

#### 3.1. A star formation history in three age bins

We use VESPA (Tojeiro et al. 2007) to model the observed spectrum of a galaxy as a linear combination of up to sixteen single stellar populations (SSPs) of different ages and metallicities shielded by a common dust screen. The resulting ages, stellar masses formed, metallicities, and dust values for roughly 800,000 individual galaxies in SDSS's Seventh Data Release (Abazajian et al. 2009) have been published in Tojeiro et al. (2009). This public database currently holds only the SDSS Main Galaxy and LRG samples; the additional Stripe 82 galaxies used in this paper will be added soon.

While VESPA recovers the star formation history in up to sixteen logarithmically spaced age bins, the number and temporal width of these bins vary according to the quality of a given galaxy's spectrum. VESPA's analysis and solutions are also model-dependent, particularly for recent star formation (Tojeiro et al. 2009). The recovered mass of stars formed in the most recent age bins, more recently than 70 Myr ago (in the rest-frame of the galaxy) with our choice of bins, is particularly sensitive to the dust modeling. The mass formed in the next group of age bins, between 70 and 420 Myr, is sensitive to the choice of SSP (see Figures 15 and 20 of Tojeiro et al. 2009). To deal with these limitations, we:

- select the stellar models that give the most physically reasonable answer, and
- limit our recovered star formation histories to three age bins.

Over a typical ensemble of galaxies, the recovered star formation rate from 70 to 420 Myr is anticorrelated with and significantly lower than the rate up to 70 Myr. The difficulty of determining the abundance of a few hundred Myr old stars in the presence of very recent star formation is less pronounced with the Maraston (2005) SSP models. To limit the impact of this, we combine all age bins younger than 420 Myr into a single bin. With these choices, the recovered star formation rate becomes a smooth function of lookback time. We seek the star formation histories of all galaxies in the same bins, and therefore degrade the age bins older than 420 Myr into two broad bins. We thus recover the star formation histories for all galaxies in the three age bins detailed in Table 1. For each galaxy, we obtain the stellar mass

<sup>7</sup> <http://www.cfa.harvard.edu/iau/lists/Supernovae.html>

TABLE 1  
THE THREE VESPA AGE BINS.

Bin	Age Range (Gyr)	MS Spectral Types <sup>a</sup>
1	0.002 – 0.42	O and B
2	0.42 – 2.4	A
3	2.4 – 14	F and later

<sup>a</sup> The main sequence (MS) spectral types that dominate the galaxy spectra in this age range.

formed over each age range, the mass-weighted metallicity in each bin, and an average value for the optical depth of interstellar dust.

The boundaries between the age bins in Table 1 are chosen for convenience and to correspond to the main sequence lifetimes of stellar spectral classes: we take them as given and estimate stellar masses. This does not imply that the exact age boundaries have any physical significance; they are simply logarithmically spaced divisions.

### 3.2. Stretch measurements

We have refitted all the light curves from SDSS-SN (§2) with the SALT II algorithm (Guy et al. 2007). This template-based routine takes the redshift and all measured fluxes in several bands as input, and performs a four-parameter fit. We fit to the SDSS-SN light curves in the  $g$ ,  $r$ , and  $i$  bands. We exclude the  $u$  band data from all analyses because of its poor signal-to-noise ratio, and exclude the  $z$  band data because Type Ia near-infrared light curves are often double-peaked and poorly fit by the SALT II templates. The SALT II outputs consist of a stretch-like parameter ( $x_1$  in Guy et al. 2007), color  $c$  ( $B - V$  at  $B$  band maximum relative to Guy et al.’s sample average), rest-frame peak  $B$  magnitude  $m_B$ , and time of maximum light. For this work, we convert  $x_1$  back to the traditional stretch  $s$  using the relation given in Guy et al. (2007):

$$s = 0.98 + 0.091x_1 + 0.003x_1^2 - 0.00075x_1^3. \quad (3)$$

Stretch  $s$  is a dimensionless parameter that describes the temporal width of the Type Ia light curve relative to a fiducial average. In our sample,  $s$  ranges from 0.70 to 1.31 with a median of 0.94. The color parameter  $c$  is a degenerate combination of host galaxy extinction and intrinsic color, which for our SNe ranges from  $-0.14$  to 0.90 with a median of 0.06.

While SALT II estimates the errors of all of its fitted parameters, we have assigned subjective quality ratings to each object as an independent error metric, based on our confidence in the best-fit value of the stretch parameter  $s$ . We have excluded objects with poorly determined stretches (32 of the 133 with host-galaxy spectra) from all further analysis. Four sample light curves in  $g$ ,  $r$ , and  $i$ , including one that was rejected in this fashion, are shown in Figure 1. We thus arrive at our sample of 101 SNe selected from about 77,000 control galaxies with spectra.

The selection of these 101 SNe Ia by inspection of the light curves could possibly introduce a bias in our results. To minimize the likelihood of this, we made all assessments of light curve quality blindly, with no knowledge of the host galaxy properties. Only after all of our supernova light curves were fitted and rated did we perform

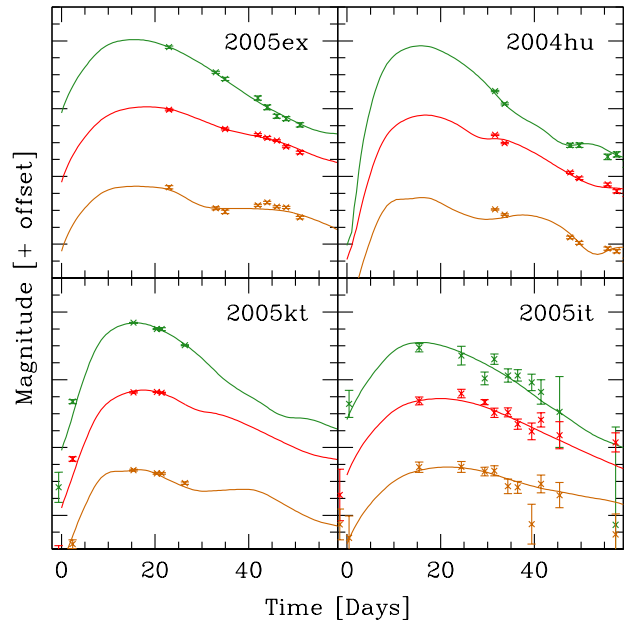


FIG. 1.— Light curves in  $g$ ,  $r$ , and  $i$  (top to bottom) for four objects with host galaxies in the SDSS spectroscopic sample; the bands are offset for clarity. The object shown in the upper right panel has little data near peak light and was therefore excluded as having an uncertain stretch. The other three objects entered our final sample of 101 SNe. Even though the object shown in the top left panel, 2005ex, has no data before maximum light, it is very well-sampled and well-fit. Because we only use these fits to divide our sample in two (§3.3), we want to maximize our sample size by including SNe like 2005ex.

any analysis on their hosts. We stress that we do not calibrate SNe as standard candles (which would require the recovery of three parameters from the light curve fit), but only use the light curves to divide our sample in two (§3.3). Because of this, our light curves need not be as well-sampled as for cosmological analyses. We present details of this final sample of 101 SNe in Table 2.

### 3.3. The High/Low Stretch Division

We wish to quantify the correlation between SN Ia stretch and host galaxy stellar populations using the VESPA analysis. Given our limited sample size, we seek to split our SNe into two populations based on their stretches. We weight each of our 101 supernovae by  $M_{i,j}$ , the stellar mass in its host galaxy  $j$  in a given VESPA age bin  $i$ . We then define the total  $M_i$  for supernovae with stretch  $s$  lying in the interval  $[a, a + \Delta s]$  (taking  $\Delta s = 0.04$ , slightly larger than a typical error in the stretch parameter) as

$$M_i(s) \equiv \sum_{s_j \in [a, a + \Delta s]} M_{i,j} \quad (4)$$

with  $j$  running over our 101 objects. This quantifies the total star formation rate in a given age bin associated with the SNe Ia in our sample. Note that  $M_{i,j}$  is equal to the mass of *possible*, not actual, SN Ia progenitor systems. Because galaxies are composed of a mix of stellar populations of different ages, we cannot derive the delay time distribution directly from these associated stellar masses.

TABLE 2  
THE RESTRICTED SDSS-SN SAMPLE

IAU ID	Host Redshift	RA (J2000) Dec <sup>a</sup>			Stretch	VESPA Host Stellar Mass ( $M_{\odot}$ )		
		h m s	° ' "			2 - 420 Myr	0.42 - 2.4 Gyr	2.4 - 14 Gyr
2004hz	0.1427	02 05 03.0	+0 50 11.9	high	$8.8 \times 10^8$	0	$1.6 \times 10^{11}$	
2004ia	0.1437	02 18 02.3	+0 33 32.4	high	$7.2 \times 10^{10}$	0	$2.6 \times 10^{11}$	
2004ie	0.0513	22 01 46.6	+1 14 12.0	high	$3.7 \times 10^7$	$9.9 \times 10^8$	$2.9 \times 10^{10}$	
2004ig	0.1830	00 05 51.8	+0 59 45.1	high	$3.2 \times 10^9$	$2.9 \times 10^{10}$	$1.4 \times 10^{11}$	
2005ed	0.0865	00 02 49.4	+0 45 04.3	low	0	$8.8 \times 10^9$	$4.0 \times 10^{11}$	
2005ef	0.1077	00 58 22.9	+0 40 44.4	low	$3.5 \times 10^8$	$9.5 \times 10^9$	$3.4 \times 10^{11}$	
2005eg	0.1914	01 02 08.5	+0 52 44.4	high	$1.5 \times 10^9$	$4.6 \times 10^{10}$	$3.8 \times 10^{11}$	
2005ex	0.0935	01 41 51.2	+0 51 35.0	high	$1.8 \times 10^9$	0	$1.7 \times 10^{11}$	
2005ez	0.1298	03 07 11.0	+1 07 10.4	low	$3.4 \times 10^9$	0	$1.5 \times 10^{11}$	
2005fa	0.1615	01 39 36.1	+0 45 31.5	high	0	$1.9 \times 10^{10}$	$6.3 \times 10^{11}$	
2005fh	0.1190	23 17 29.7	+0 25 45.8	high	0	$4.9 \times 10^{10}$	$2.0 \times 10^{11}$	
2005fv	0.1181	03 05 22.4	+0 51 30.1	high	$4.4 \times 10^8$	$4.7 \times 10^{10}$	$2.5 \times 10^{11}$	
2005gb	0.0864	01 16 12.6	+0 47 31.0	low	$4.3 \times 10^8$	$1.3 \times 10^{10}$	$3.7 \times 10^{11}$	
2005gh	0.2591	20 50 36.4	+0 21 14.8	high	$1.3 \times 10^9$	$7.4 \times 10^{10}$	$7.5 \times 10^{11}$	
2005gp	0.1266	03 41 59.3	+0 46 57.6	low	$7.4 \times 10^8$	$4.6 \times 10^9$	$7.3 \times 10^{10}$	
2005hc	0.0459	01 56 47.9	+0 12 49.2	high	0	$7.4 \times 10^9$	$3.9 \times 10^{11}$	
2005hj	0.0574	01 26 48.3	-1 14 16.8	high	$9.8 \times 10^7$	$6.0 \times 10^8$	$1.9 \times 10^{10}$	
2005hn	0.1085	21 57 04.2	+0 13 24.5	low	$6.2 \times 10^8$	0	$1.1 \times 10^{10}$	
2005ho	0.0628	00 59 24.1	+0 00 09.4	high	$2.3 \times 10^9$	0	$2.3 \times 10^{10}$	
2005if	0.0670	03 30 12.9	+0 58 28.5	low	$3.1 \times 10^9$	0	$1.1 \times 10^{11}$	
2005ij	0.1245	03 04 21.3	-1 03 46.6	high	$2.7 \times 10^9$	$2.0 \times 10^{10}$	$1.2 \times 10^{11}$	
2005ir	0.0763	01 16 43.8	+0 47 40.4	high	$3.1 \times 10^9$	$9.3 \times 10^9$	$2.9 \times 10^{11}$	
2005je	0.0939	02 35 26.6	+1 04 29.6	low	0	$1.9 \times 10^{10}$	$8.1 \times 10^{11}$	
2005js	0.0796	01 34 41.5	+0 36 19.3	low	0	$1.1 \times 10^{10}$	$5.7 \times 10^{11}$	
2005kt	0.0653	01 10 58.0	+0 16 34.1	low	0	$1.9 \times 10^{10}$	$1.3 \times 10^{11}$	
2005ku	0.0454	22 59 42.6	+0 00 49.3	high	$3.0 \times 10^9$	0	$5.3 \times 10^{10}$	
2005lj	0.0777	01 57 43.0	+0 10 46.0	high	$5.9 \times 10^8$	0	$5.2 \times 10^{10}$	
2005lk	0.1042	21 59 49.4	-1 11 37.3	low	$7.1 \times 10^8$	$4.0 \times 10^{10}$	$7.9 \times 10^{11}$	
2006eq	0.0494	21 28 37.1	+1 13 41.2	low	$9.4 \times 10^7$	$8.3 \times 10^9$	$2.1 \times 10^{11}$	
2006er	0.0843	00 21 37.5	-1 00 35.9	low	0	$1.0 \times 10^{10}$	$5.0 \times 10^{11}$	
2006ex	0.1472	20 38 43.9	+0 28 28.3	high	$1.3 \times 10^9$	$1.1 \times 10^{11}$	$2.7 \times 10^{11}$	
2006fb	0.2451	23 35 51.5	+0 10 37.6	high	$1.0 \times 10^9$	$4.2 \times 10^{10}$	$3.6 \times 10^{11}$	
2006fd	0.0799	20 37 53.2	+1 13 16.1	low	0	$2.2 \times 10^{10}$	$2.6 \times 10^{11}$	
2006ff	0.2353	00 26 35.6	+0 18 07.5	high	$2.4 \times 10^9$	$6.6 \times 10^9$	$3.2 \times 10^{11}$	
2006fi	0.2306	22 19 50.3	+0 01 27.8	high	$4.1 \times 10^9$	$5.8 \times 10^{10}$	$2.3 \times 10^{11}$	
2006fl	0.1717	22 11 27.7	+0 45 21.5	high	$8.7 \times 10^8$	$9.1 \times 10^9$	$6.2 \times 10^{10}$	
2006fs	0.0991	21 09 59.0	+0 24 31.6	high	$2.3 \times 10^9$	$2.1 \times 10^{10}$	$4.1 \times 10^{11}$	
2006fu	0.1985	23 51 08.4	+0 44 46.9	high	$1.5 \times 10^9$	$2.5 \times 10^8$	$4.0 \times 10^{10}$	
2006fv	0.1319	01 21 37.9	+0 24 52.2	low	0	$8.9 \times 10^9$	$5.0 \times 10^{11}$	
2006fy	0.0827	23 26 40.2	+0 50 24.9	high	$2.5 \times 10^9$	$1.2 \times 10^9$	$3.5 \times 10^{10}$	
2006fz	0.1047	00 16 41.4	+0 25 28.3	low	0	$2.1 \times 10^{10}$	$9.6 \times 10^{11}$	
2006gb	0.2660	23 59 16.5	-1 15 01.3	low	$4.5 \times 10^9$	$6.5 \times 10^{10}$	0	
2006gx	0.1807	02 48 14.1	+0 20 49.3	high	$6.5 \times 10^9$	$8.7 \times 10^9$	$5.3 \times 10^{10}$	
2006hd	0.2983	21 44 03.5	+0 43 34.6	high	$2.0 \times 10^9$	$2.9 \times 10^{10}$	$6.7 \times 10^{10}$	
2006hh	0.2374	02 42 27.0	+0 47 38.9	low	$2.9 \times 10^8$	$6.9 \times 10^{10}$	$1.2 \times 10^{12}$	
2006hr	0.1576	01 50 15.6	+0 53 14.1	high	$1.4 \times 10^{10}$	0	$8.4 \times 10^{10}$	
2006hw	0.1394	03 13 03.4	+0 28 17.9	high	$2.4 \times 10^{10}$	0	$3.9 \times 10^{11}$	
2006hx	0.0454	01 13 57.3	+0 22 18.0	high	$1.3 \times 10^8$	$1.6 \times 10^{10}$	$1.6 \times 10^{11}$	
2006ia	0.1749	02 07 19.2	+1 15 07.5	low	$1.5 \times 10^8$	$4.5 \times 10^{10}$	$1.9 \times 10^{12}$	
2006ib	0.1811	03 16 11.8	+0 36 03.4	low	0	0	$1.4 \times 10^{11}$	
2006ju	0.1486	23 24 39.0	+0 43 06.0	low	$3.5 \times 10^9$	$4.1 \times 10^{10}$	$8.4 \times 10^{11}$	
2006jw	0.2495	02 23 22.3	+0 49 08.4	high	$9.7 \times 10^8$	$8.1 \times 10^{10}$	$2.4 \times 10^{11}$	
2006jz	0.1994	00 11 24.8	+0 42 09.8	low	0	$1.1 \times 10^{11}$	$1.7 \times 10^{12}$	
2006kd	0.1363	01 07 50.0	+0 49 41.5	high	$7.7 \times 10^8$	0	$1.2 \times 10^{11}$	
2006kq	0.1983	21 15 36.6	+0 19 17.1	high	$2.0 \times 10^9$	$4.0 \times 10^{10}$	$1.4 \times 10^{11}$	
2006kw	0.1854	02 14 58.0	+0 36 09.0	high	$9.6 \times 10^9$	0	$6.2 \times 10^{10}$	
2006kx	0.1599	03 42 14.7	+0 28 41.8	high	$4.8 \times 10^7$	$8.2 \times 10^9$	$5.5 \times 10^{10}$	
2006lb	0.1819	03 19 28.2	+0 19 04.9	high	$3.0 \times 10^9$	$8.3 \times 10^9$	$5.1 \times 10^{10}$	
2006nd	0.1288	22 44 59.1	-1 00 23.8	high	$2.4 \times 10^{10}$	0	$5.5 \times 10^{11}$	
2006ne	0.0466	01 13 37.8	+0 25 25.9	low	$1.6 \times 10^9$	$1.1 \times 10^{10}$	$1.7 \times 10^{11}$	
2006ni	0.1750	20 54 52.4	+0 11 41.4	low	0	$6.0 \times 10^{10}$	$9.3 \times 10^{11}$	
2006nn	0.1969	01 45 41.0	-1 03 15.8	high	$1.3 \times 10^9$	0	$1.3 \times 10^{11}$	
2006nz	0.0381	00 56 29.2	-1 13 36.1	low	0	$1.6 \times 10^9$	$7.6 \times 10^{10}$	
2006oa	0.0625	21 23 42.9	+0 50 36.5	high	0	$1.7 \times 10^7$	$8.8 \times 10^7$	
2006ob	0.0592	01 51 48.1	+0 15 48.3	low	0	$2.1 \times 10^{11}$	$8.8 \times 10^{11}$	
2006ol	0.1191	23 28 07.2	+0 51 22.9	low	0	$3.3 \times 10^{10}$	$1.1 \times 10^{12}$	

TABLE 2—Continued

IAU ID	Host Redshift	RA (J2000) Dec <sup>a</sup>			Stretch	VESPA Host Stellar Mass ( $M_{\odot}$ )		
		h m s	° ' "	° ' "		2 - 420 Myr	0.42 - 2.4 Gyr	2.4 - 14 Gyr
2006on	0.0719	21 55 58.5	-1 04 12.7	high	0	$9.8 \times 10^9$	$4.7 \times 10^{10}$	
2006op	0.0341	21 21 31.9	+0 59 35.9	low	$2.4 \times 10^8$	$3.7 \times 10^9$	$2.8 \times 10^{10}$	
2006pe	0.1611	00 23 09.2	+0 03 13.1	low	0	$3.1 \times 10^{10}$	$1.1 \times 10^{12}$	
2006py	0.0578	22 41 42.0	+0 08 12.9	low	0	$3.1 \times 10^9$	$9.5 \times 10^{10}$	
2007ht	0.0727	00 34 33.8	-1 13 03.1	low	$1.4 \times 10^8$	$1.6 \times 10^{10}$	$6.8 \times 10^{11}$	
2007hx	0.0794	02 06 27.1	+0 53 58.3	high	$5.4 \times 10^9$	$1.8 \times 10^{10}$	$3.4 \times 10^{11}$	
2007hy	0.1814	03 39 42.3	+1 05 32.2	high	0	$2.2 \times 10^{10}$	$5.3 \times 10^{11}$	
2007hz	0.1393	21 03 08.9	-1 01 45.1	high	$7.1 \times 10^9$	0	$6.7 \times 10^{11}$	
2007ia	0.1310	03 43 10.1	+0 06 08.9	low	$1.6 \times 10^9$	$6.0 \times 10^{10}$	$5.1 \times 10^{11}$	
2007id	0.1603	21 46 00.5	-1 13 03.9	high	0	$4.2 \times 10^9$	$1.8 \times 10^{11}$	
2007ie	0.0934	22 17 36.7	+0 36 48.0	low	$7.9 \times 10^8$	0	0	
2007jk	0.1829	02 55 05.6	+0 08 50.8	high	$3.7 \times 10^8$	$6.3 \times 10^9$	$1.3 \times 10^{11}$	
2007js	0.1464	20 36 48.7	+0 05 54.4	high	$9.4 \times 10^9$	0	0	
2007jt	0.1447	02 28 32.8	-1 02 31.6	low	$1.7 \times 10^9$	$1.8 \times 10^{10}$	$9.0 \times 10^{10}$	
2007kl	0.2571	02 44 50.9	+0 21 53.4	high	$9.6 \times 10^8$	$5.7 \times 10^{10}$	$8.5 \times 10^{11}$	
2007kv	0.3295	01 10 15.8	+0 28 19.3	high	$3.6 \times 10^8$	$3.3 \times 10^{10}$	$3.0 \times 10^{11}$	
2007lr	0.1562	00 49 00.3	+0 19 26.4	high	$6.1 \times 10^8$	$2.9 \times 10^{10}$	$7.3 \times 10^{11}$	
2007ma	0.1073	00 44 53.8	+0 59 49.3	high	$1.6 \times 10^9$	$6.5 \times 10^9$	$5.4 \times 10^{10}$	
2007mh	0.1278	03 14 31.8	+0 16 11.4	high	$8.9 \times 10^8$	0	$4.5 \times 10^{10}$	
2007mi	0.1322	03 23 31.5	+0 39 60.0	low	0	$1.6 \times 10^{10}$	$5.2 \times 10^{11}$	
2007mj	0.1232	03 34 44.4	+0 21 19.9	high	$2.5 \times 10^8$	$2.5 \times 10^{10}$	$1.5 \times 10^{11}$	
2007mm	0.0665	01 05 46.7	+0 45 31.8	low	0	$1.5 \times 10^9$	$6.8 \times 10^{10}$	
2007mn	0.0769	02 05 04.0	+0 10 28.4	high	$2.8 \times 10^9$	$3.7 \times 10^{10}$	$4.4 \times 10^{11}$	
2007nj	0.1540	02 52 27.4	+0 15 06.6	low	$4.7 \times 10^9$	$1.7 \times 10^{10}$	$3.8 \times 10^{11}$	
2007ok	0.1655	02 28 24.3	+0 11 04.8	high	$3.0 \times 10^8$	$3.6 \times 10^{10}$	$4.3 \times 10^{11}$	
2007ol	0.0560	01 37 23.7	+0 18 43.2	low	0	$7.4 \times 10^9$	$1.7 \times 10^{11}$	
2007om	0.1052	23 54 20.7	+0 55 03.4	high	$3.9 \times 10^8$	$7.9 \times 10^{10}$	$7.6 \times 10^{11}$	
2007ou	0.1132	02 23 42.7	+0 49 33.6	high	$2.2 \times 10^9$	0	$1.2 \times 10^{11}$	
2007ph	0.1294	20 51 13.4	+0 57 20.9	low	0	$1.1 \times 10^{10}$	$9.2 \times 10^{11}$	
2007pt	0.1752	02 07 38.5	+0 19 26.4	high	$1.8 \times 10^9$	0	$7.6 \times 10^{10}$	
2007px	0.1080	00 22 44.0	+0 28 44.4	high	$2.6 \times 10^{10}$	0	$5.3 \times 10^{11}$	
2007py	0.2094	03 29 31.6	+0 30 56.0	low	$1.6 \times 10^9$	0	$1.3 \times 10^{11}$	
2007qa	0.1085	01 52 33.9	+1 14 38.7	high	$1.6 \times 10^9$	0	$1.3 \times 10^{11}$	
2007qr	0.1359	02 52 29.2	-1 08 22.3	high	$6.0 \times 10^8$	$1.4 \times 10^9$	$5.7 \times 10^{10}$	
2007rs	0.1241	00 46 27.4	-1 03 44.1	low	0	$6.6 \times 10^{10}$	$1.8 \times 10^{12}$	

<sup>a</sup> Position of SN; data available from <http://www.cfa.harvard.edu/iau/lists/Supernovae.html> and <http://www.cfa.harvard.edu/iau/cbat.html>.

With this caveat in mind, the resulting distributions of stellar mass as a function of stretch in different mass bins are shown in Figure 2. The top panel is a histogram of stretches, while the second, third, and fourth panels weight each SN by its host stellar mass in young, middle, and old age bins, respectively. The second and fourth panels, in particular, show that lower stretch SNe live in hosts with large quantities of old stars but little recent star formation, while higher stretch SNe are in hosts with abundant recent star formation. Given the rough bimodality shown here, we call Type Ia supernovae *high stretch* if they have  $s > 0.92$ , and *low stretch* otherwise. In SDSS-SN, this division yields 60 high stretch and 41 low stretch SNe; the binnings are listed in Table 2.

This result confirms the work of Sullivan et al. (2006), Neill et al. (2009), Gallagher et al. (2005), and others: that high stretch SNe are associated with star-forming galaxies. We now seek to study this association in more detail and to derive a quantitative delay time distribution for high and low stretch SNe Ia.

### 3.4. Average Spectra

The difference in stellar populations indicated by Figure 2 should manifest itself in the spectra of the hosts. To examine this, we constructed average spectra of the high stretch and low stretch hosts. We corrected the spectra for Milky Way extinction using the dust maps of Schlegel et al. (1998) and a Fitzpatrick (1999)  $R_V = 3.1$  extinction law. We scaled each spectrum to a common  $r$  band fiber magnitude, shifted the spectra to  $z = 0$ , masked bad pixels flagged by the SDSS pipeline, and weighted by the inverse variance in coadding. To obtain robust estimates of the mean and variance of the average spectra, we have used bootstrap resampling on the samples of 60 high stretch and 41 low stretch hosts.

The results, shown in Figure 3, are striking. The average spectrum of a high stretch host shows exceptionally strong nebular emission lines such as the Balmer series, [OIII], [OII], [NII], and [SII] and a strong blue continuum, all clearly indicative of recent and ongoing star formation. The average spectrum of low stretch supernova hosts, by contrast, shows absorption lines characteristic of old stellar populations and little evidence of interstellar gas. The difference spectrum (lower panel) looks much like the spectrum of a main-sequence B type star with nebular emission lines superimposed. Intriguingly, a single B3 spectrum from Silva & Cornell (1992) fits the continuum and absorption lines of the difference spectrum better than models of either a 50 Myr-old single stellar population, or 400 Myr of continuous star formation. While the bootstrap errors are too large to exclude either of these possibilities, Figure 3 tantalizingly suggests very young progenitors for some SNe Ia, as the difference spectrum appears to require a population  $\lesssim 50$  Myr old (B3 stars live for about 30 Myr). Note that we cannot be absolutely certain that the progenitors are this young, if bursts of star formation typically last long enough so that a somewhat older population is likely to be associated with ongoing star formation.

Figure 3 confirms the difference in host galaxies indicated in Figure 2 by the VESPA-derived star formation histories. High stretch, luminous Type Ia's are associated with young O and B stars, while lower stretch SNe are found in galaxies with much older stellar populations.

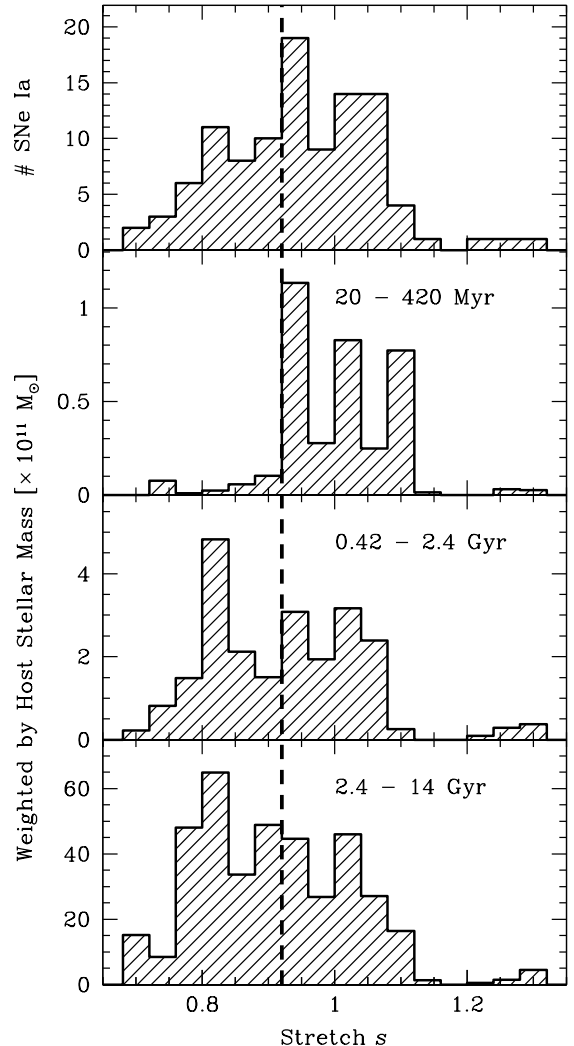


FIG. 2.— Histograms of stellar mass of supernovae Ia hosts binned by SN stretch. Objects in the top panel are unweighted, while SNe in the lower three panels are weighted by the stellar mass of their host galaxy in young (top), middle-aged (middle) and old (bottom) stars. SNe with  $s \gtrsim 0.92$  (to the right of the dotted line) are associated with young stars, while lower stretch SNe are not. To further explore this distinction, we define supernovae with  $s > 0.92$  as *high stretch* SNe Ia.

Figure 3 offers a clear and dramatic confirmation of the association between high stretch SNe and star formation. The average spectra change imperceptibly when the high/low stretch boundary is varied from 0.90 to 0.92, representing a typical stretch error as reported by SALT II. Our results are therefore unlikely to be affected by measurement errors in the stretch parameter.

## 4. TOWARDS A DTD

While Figure 3 is compelling on its own, we can do better. With a well-controlled survey, spectra for all galaxies in the control sample, and VESPA star formation histories for all of these galaxies, we now seek to calculate a delay time distribution in the three age bins of Table 1. We do not assume any functional form for the efficiency of making SNe as a function of progenitor age, but simply see what constraints the data alone can provide.

Our method is as follows:

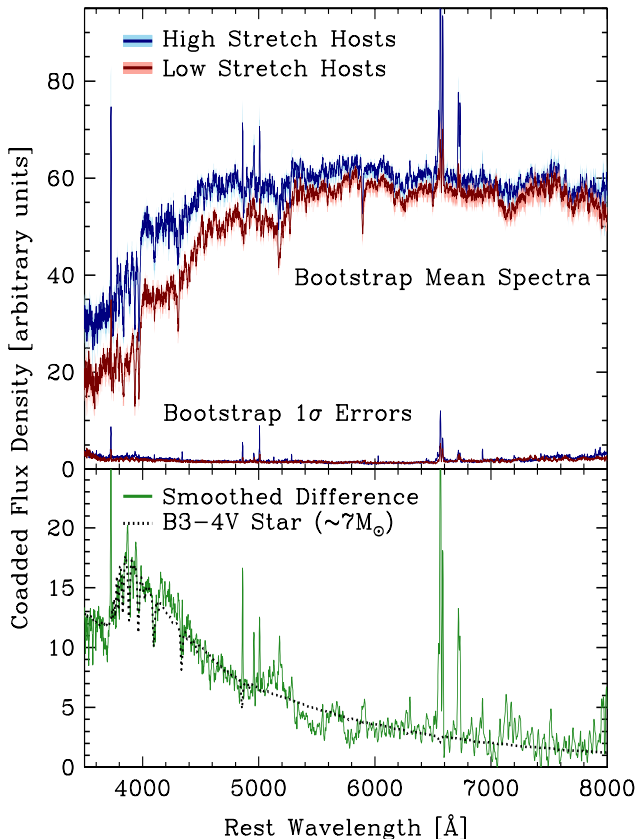


FIG. 3.— Coadded SDSS spectra of hosts of 60 high stretch ( $s > 0.92$  - blue) and 41 low stretch ( $s < 0.92$  - red) supernovae (upper panel); the shading shows the  $1\sigma$  error range derived from bootstrap resampling. Note the strong blue continuum and nebular emission lines, indicative of recent and ongoing star formation, in the high stretch hosts. The low stretch host spectrum has features characteristic of much older stellar populations. The difference (lower panel) looks remarkably similar to the spectrum of a typical B star (note the strong Balmer series in absorption), suggesting young progenitors for high stretch Type Ia SNe. The stellar spectrum is from Silva & Cornell (1992).

1. Parametrize the DTD as an explosion rate per unit stellar mass  $\epsilon_i$  for stars in each of three age bins  $i$ ,
2. Assume a prior probability distribution on the DTD explosion rates,
3. Select DTDs from this prior,
4. Generate samples of mock hosts from the DTDs and VESPA star formation histories of our control sample,
5. Compare the average spectra of the mock hosts and observed hosts to calculate a likelihood for each DTD realization,
6. Repeat steps 3 - 5 many times to explore the  $\epsilon_i$  space and obtain a posterior probability distribution on the DTD.

We now discuss the general form of the delay time distribution and then each of these steps.

#### 4.1. The Delay Time Distribution

Our star formation histories consist of the total stellar mass formed in each of three age bins for each host galaxy. The most general delay time distribution is therefore a set of three efficiencies,  $\epsilon_i$ , representing the mean number of SNe per unit stellar mass per year from progenitors in age bin  $i$  (Table 1). We treat high stretch and low stretch SNe separately in this analysis, giving two sets of efficiencies  $\epsilon_{h,i}$  and  $\epsilon_{l,i}$ .

We may effectively remove two of these six parameters by requiring that the sets of efficiencies be appropriately normalized, i.e. that the total number of expected SNe times their probability of detection equal the number of SNe observed,

$$N_{SN,h} = \sum_{\text{gals } j} p_{h,j}(\text{detect}) t \sum_i \epsilon_{h,i} M_{i,j}, \quad (5)$$

where  $p_{h,j}(\text{detect})$  is the probability that a supernova of high stretch in galaxy  $j$  enters the sample,  $M_{i,j}$  is the amount of stellar mass formed in age bin  $i$  in galaxy  $j$ ,  $N_{SN,h}$  is the number of high stretch SNe Ia observed, and  $t$  is the duration of the survey. An identical constraint applies to low stretch supernovae.

For future use, we also introduce normalized explosion efficiencies corresponding to the fraction of high or low stretch supernovae produced by stars in a given age bin, e.g.

$$\epsilon'_{h,i} \equiv \epsilon_{h,i} \frac{1}{N_{SN,h}} \sum_{\text{gals } j} p_{h,j}(\text{detect}) M_{i,j}. \quad (6)$$

Thus,  $\epsilon'_{h,i}$  and  $\epsilon'_{l,i}$  each sum to unity.

#### 4.2. Priors

In order to use a Bayesian analysis to constrain the  $\epsilon_{h,i}$  and  $\epsilon_{l,i}$ , we need to choose a prior distribution. Following Laplace (1814) and general practice in the literature, we seek a uniform prior. However, due to the normalization constraint, we cannot place uniform priors simultaneously on all of the  $\epsilon_{h,i}$  or  $\epsilon_{l,i}$ . An alternative would be to choose our priors to be uniform in area over the two dimensional plane defined by Equation (5). However, the projection of this prior onto any of the  $\epsilon'_{h,i}$  yields a probability distribution strongly peaked towards low values. Physically, this biases us against a DTD in which one age bin is responsible for a large fraction of the SNe (see Figure 4). To avoid these combinatorial effects, we use a Monte Carlo sampling that places a uniform prior on *one* of the  $\epsilon'_{h,i}$  and *one* of the  $\epsilon'_{l,i}$  in each realization. By choosing  $i$  randomly in each iteration, we retain the symmetry between all of the  $\epsilon'_{h,i}$  and  $\epsilon'_{l,i}$ .

We note that there are many possible priors that look qualitatively similar to that shown in Figure 4. We do not argue that our choice is optimal, only that it is reasonable. We have also tested the dependence of our constraints on the choice of prior and found little variation, as long the prior probability density does not approach zero for any values of  $\epsilon'_i$ .

#### 4.3. Creating a Mock Sample

Given a model delay time distribution (i.e., sets of  $\epsilon_{h,i}$  and  $\epsilon_{l,i}$ ), we compute the expected number of high and



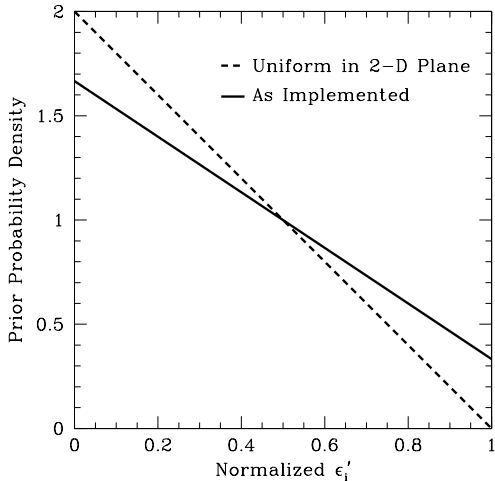


FIG. 4.— Projected prior distributions for each  $\epsilon'_i$ , the fraction of high/low stretch SNe with progenitors in age bin  $i$ . The normalized  $\epsilon'_i$  are related to the physical explosion rates  $\epsilon_i$  by Equation (6). A prior uniform in the 2-D plane defined by Equation (5) would be strongly biased against DTDs concentrated in one age bin.

low stretch supernovae ( $\ll 1$ ) observed in each galaxy in the control sample. For a galaxy  $j$ , this is the sum of the explosion efficiencies times the mass in each stellar age bin weighted by the detection probability:

$$\langle n_{SN,h,j} \rangle = p_{h,j}(\text{detect}) \sum_i \epsilon_{h,i} M_{i,j}. \quad (7)$$

Our code thus generates realizations of  $\{\epsilon'_i\}$  for both high and low stretch, converts to  $\{\epsilon_i\}$  using Equation (6), and computes the number of SNe Ia in each control galaxy as a Poisson random number with a mean given by Equation (7).

For the detection probability, we use a crude estimate of the selection function and tweak the parameters to match the approximate redshift range of the subset of SDSS-SN with host galaxy spectra. We adopt the functional form

$$p(\text{detect}) = \left[ 1 + \exp\left(\frac{m_{\text{peak}} - m_{\text{lim}}}{a}\right) \right]^{-1}, \quad (8)$$

where  $m_{\text{peak}}$  is the supernova's peak SDSS  $r$  band magnitude,  $m_{\text{lim}}$  is an approximate limiting magnitude of the survey, and  $a$  is a softening parameter to account for the dispersion in SN peak magnitudes and colors and the survey detection efficiency. Because this model does not naturally capture the fact that higher stretch SNe are above any threshold for a longer period of time, we allow the parameters  $m_{\text{lim}}$  and  $a$  to differ for high and low stretch objects. Fitting to the observed redshift distribution, we adopt  $m_{\text{lim}} = 19.5$  and  $a = 0.6$  for low stretch SNe, and  $m_{\text{lim}} = 20.2$  and  $a = 0.4$  for high stretch SNe. The peak supernova magnitude in  $r$  is given by

$$m_{\text{peak}} = M_{\text{stand}} - \alpha(s - 1) + \mu(z) + K(s, z) + A_r \quad (9)$$

where  $M_{\text{stand}}$  is the standardized peak B absolute magnitude,  $\alpha$  is the Phillips (1993) parameter relating stretch and peak luminosity,  $s$  is a typical stretch,  $\mu(z)$  is the distance modulus,  $A_r$  is the  $r$  band Milky Way extinction along the supernova's line of sight (Schlegel et al. 1998),

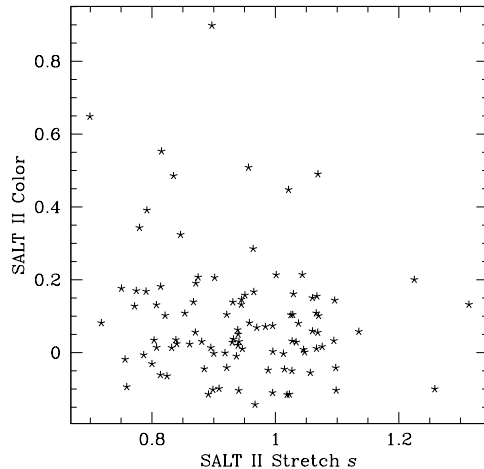


FIG. 5.— Stretch vs. color ( $B-V$  at peak  $B$  magnitude relative to a fiducial average), as determined by SALT II. The two quantities are not correlated, which allows us to fold the color variation into the detection efficiency (Equation 8).

and  $K(s, z)$  is an approximate  $K$ -correction to the SDSS  $r$  band at  $z = 0$  (see Nugent et al. (2002) for details on the  $K$ -correction). We adopt the values  $M_{\text{stand}} = -19.41$  and  $\alpha = 1.56$  (Guy et al. 2005), and take the typical values of  $s$  to be our sample medians, 1.02 for high stretch and 0.83 for low stretch SNe Ia. Since we fit for  $m_{\text{lim}}$  and  $a$  to reproduce the observed redshift distribution *after* fixing all other parameters, changing the standardized absolute magnitude  $M_{\text{peak}}$  will not affect our results. Because we fit high and low stretch SNe separately, the value of  $\alpha$  similarly has no effect. Equation (9) does not account for variation in color ( $B-V$  at peak  $B$  magnitude), which is instead absorbed into the softening parameter  $a$ . If color is correlated with stretch, Equation (9) will not fully capture differences between the detectability of high and low stretch SNe. However, as shown in Figure 5, we find no evidence of such a correlation.

Figure 6 compares the redshift distribution of a mock sample generated by Equations (7), (8), and (9) with the observed redshift distribution. While there are slight differences, the means and widths of the distributions agree reasonably well for both high and low stretch SNe. The detection probability given by Equation (8) is intended only to be approximate and to set the redshift range of galaxies that serve as potential hosts. Modest variations in Equations (8) and (9) have almost no effect on our results, particularly because we compare spectra weighted by their inverse variances: the slight discrepancy at high redshift is dominated by galaxies with poor signal-to-noise ratio spectra that have a very small impact on the average spectrum. As an additional check, we have verified that Equations (7), (8), and (9) successfully reproduce the observed range of host galaxy masses as derived from VESPA.

#### 4.4. A Likelihood Function

To use Bayes' Theorem, we need to calculate the likelihood of observed host properties given a sample of mock hosts selected with a specific model for the  $\{\epsilon_i\}$ . We use a comparison metric based on the average spectra of the

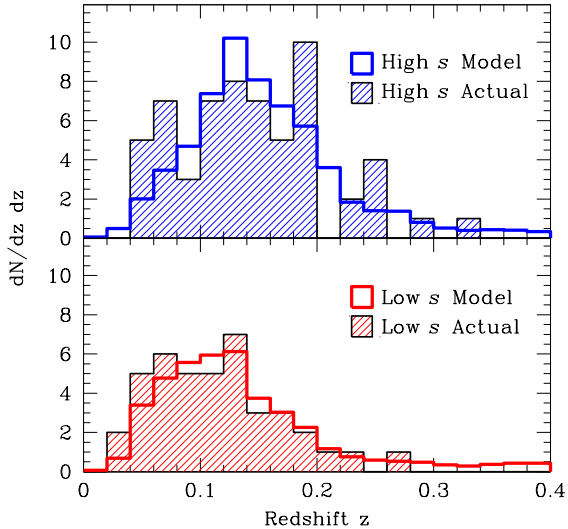


FIG. 6.— Redshift histograms of the observed SNe with SDSS host galaxy spectra against the histograms of one realization of mock hosts with the detection probability given by Equation (8). We adopt values of  $m_{lim} = 20.2$  and  $a = 0.4$  for high stretch SNe,  $m_{lim} = 19.5$  and  $a = 0.6$  for low stretch SNe.

host galaxies; essentially, with our Monte Carlo realizations of delay time distributions, we seek to reproduce the mean spectra shown in Figure 3. We use a  $\chi^2$  statistic to compare the average spectra of our Monte Carlo realizations to those of the observed hosts.

To obtain useful constraints, we need both very high signal-to-noise ratio average spectra for the mock samples, and reliable estimates of the mean and variance associated with the average spectra of the observed hosts. The first requirement is met by using a large mock sample drawn from our 77,000 control galaxies. The second problem is solved using bootstrap resampling of the 60 high stretch and 41 low stretch actual hosts, as described in §3.4 and shown in Figure 3. As a check, we compared the bootstrap errors to the error-weighted pixel-by-pixel scatter between spectra and found very good agreement.

With an average spectrum and bootstrap errors for the SN hosts, we may assign a  $\chi^2$  goodness-of-fit value to the mean spectrum of the mock hosts by averaging the  $\chi^2$  values over all pixels. We then use this reduced  $\chi^2$  to compute a rejection probability.

There are two reasons why we have not directly compared the stellar populations of SN Ia hosts and non-hosts. First, such a comparison would require us to apply VESPA to the SN hosts to derive their star formation histories. We are limited by  $\sqrt{N}$  statistics in the hosts, and errors in the VESPA outputs are much larger than in the spectra. Second, the recovered stellar masses would be used twice for the control galaxies: once to determine how many supernovae to set off in the mock samples (Equation 7), and once to compare the resulting mock hosts to the observed hosts. Any metric would therefore contain the sum of the squares of the recovered stellar masses, so that random variances in these masses would *add* and produce a bias. Our chosen metric, by combining spectra rather than derived quantities, avoids both drawbacks.

## 5. RESULTS

We have run 100,000 Monte Carlo realizations of the delay time distribution from the prior shown in Figure 4. In each realization, we draw a set of normalized explosion efficiencies ( $\epsilon'$ , Equation 6), convert to the physical explosion efficiencies ( $\epsilon$ , Equation 5), and use Equations (7), (8), and (9) to generate a sample of mock hosts. We then construct the composite spectra for the mock high stretch and low stretch hosts and compare them to the spectra of observed hosts shown in Figure 3 using a  $\chi^2$  test. We take the likelihood of each realization to be the rejection probability ( $Q$  function) of its computed value of  $\chi^2$ . In practice, our best-fit models do produce formally good fits, with  $\chi^2$  per pixel typically in the range 0.65 - 1.05. Normalizing these likelihoods by their sum over all Monte Carlo realizations, we obtain the posterior probability distributions for the explosion efficiencies. The distribution for a single efficiency is computed by integrating over the other variables.

The resulting probability distributions are shown in Figure 7. The lower horizontal axes give the explosion efficiencies in physical units ( $\epsilon_{h,i}$  and  $\epsilon_{l,i}$ , Equation 5), while the upper axes show the fraction of all SNe Ia in the SDSS spectroscopic sample formed as high or low stretch from a given progenitor age bin. These are computed from the  $\epsilon_{h,i}$  or  $\epsilon_{l,i}$  as, e.g.,

$$f_{h,i} = \frac{\epsilon_{h,i}}{N_{SN}} \sum_{\text{gals } j} p_{h,j}(\text{detect}) M_{i,j}, \quad (10)$$

where  $p_{h,j}(\text{detect})$  is the detection probability for high stretch SNe Ia in galaxy  $j$ ,  $M_{i,j}$  is the stellar mass formed in age bin  $i$  in galaxy  $j$ ,  $N_{SN}$  is the total (high and low stretch) number of SNe detected, and the sum is taken over control galaxies. Equation (10) differs from Equation (6) only in the denominator: while  $\epsilon'_{h,i}$  and  $\epsilon'_{l,i}$  each sum to unity,  $f_{h,i}$  and  $f_{l,i}$  together sum to unity. Note that because a volume-limited sample of galaxies will have different properties from the SDSS spectroscopic sample (in particular lower masses),  $f_{h,i}$  or  $f_{l,i}$  for the full sample of SDSS supernovae may differ from the values we recover.

These same quantities,  $f$  and  $\epsilon$ , are also plotted in Figure 8, with the top panel showing the supernova rate in physical units ( $\epsilon_{h,i}$  in blue and  $\epsilon_{l,i}$  in red) and the bottom panel showing the fraction of SNe from a given range of progenitor ages ( $f_{h,i}$  in blue and  $f_{l,i}$  in red). The dots show the median values, while the colored and black bars represent the 68% and 95% confidence intervals, respectively. For distributions peaked near zero, only upper limits and one-sided confidence intervals are shown. The constraints on  $f$  and  $\epsilon$  are also listed in Table 3.

The results are striking. We can constrain most high stretch SNe Ia to have progenitors younger than  $\lesssim 400$  Myr, and Figure 3 tantalizingly suggests an even younger characteristic age (B3 stars live for  $\sim 30$  Myr). While young stars dominate the production of high stretch SNe Ia, they make no significant contribution to the low stretch rate. Instead, these supernovae have a characteristic delay time of at least 2-3 Gyr. Intermediate progenitors, evolving on the time scale of a Main Sequence A star, contribute little to either the high or low stretch rate. In the SDSS Stripe 82 galaxies, the prompt, high

TABLE 3  
THE DTD: RESULTS OF THE MONTE CARLO

Age Range (Gyr)	$\epsilon_h^a$	$f_h^b$	$\epsilon_l^a$	$f_l^b$
0.002 – 0.42	$75^{+16}_{-16}$	$0.25^{+0.05}_{-0.05}$	$< 13$	$< 0.04$
0.42 – 2.4	$< 13$	$< 0.20$	$< 2.2$	$< 0.04$
2.4 – 14	$< 0.48$	$< 0.18$	$1.58^{+0.06}_{-0.12}$	$0.58^{+0.02}_{-0.03}$

NOTE. — The errors given are 95% confidence intervals.

<sup>a</sup> Defined in Equation (5), units are  $10^{-14}$  SNe  $M_\odot^{-1}$  yr $^{-1}$ .

<sup>b</sup> Defined in Equation (10).

stretch channel and the delayed, low stretch channel each account for roughly half of all Type Ia supernovae.

The formal constraints we obtain for the low stretch rate from young stars (Figure 7) are especially stringent. Because even blue galaxies have lots of old stars, we find it difficult to reproduce a spectrum as quiescent as that shown in Figure 3: a sample selected purely by old stellar mass will still include star-forming galaxies. Our measured spectra are *only* consistent with a delay time distribution in which all (or nearly all) low stretch SNe Ia are produced by old stars. Nevertheless, we cannot rule out any progenitor channel expected to produce  $\lesssim 1$  detectable supernova over the entire population of SDSS galaxies, and we have therefore set a floor on our SN rate constraints from Poisson statistics. This floor determines the limits on  $\epsilon_{l,1}$  and  $\epsilon_{l,2}$ , the low stretch rates from young and middle-aged stars, in Table 3 and Figure 8.

To compare our results with earlier work based on the  $A + B$  model (Equation 1), we need to interpret  $A$  and  $B$  in our framework. We take  $A$ , the coefficient of the total stellar mass, to be our supernova rate for old stars,  $\epsilon_3$ . We convert  $B$ , the coefficient of current star formation (in SNe  $M_\odot^{-1}$ ), to our rate for young stars  $\epsilon_1$  (in SNe  $M_\odot^{-1}$  yr $^{-1}$ ) by multiplying by the temporal width of our first age bin, about 400 Myr. Our results agree reasonably well with those of Neill et al. (2006) (young  $\epsilon_1 = 200 \pm 50$ , old  $\epsilon_3 = 1.4 \pm 1.0$  in our units of  $10^{-14}$  SNe  $M_\odot^{-1}$  yr $^{-1}$ ), but less well with those of Sullivan et al. (2006) ( $\epsilon_1 = 100 \pm 20$ ,  $\epsilon_3 = 5.3 \pm 1.0$ ) or Mannucci et al. (2005) ( $\epsilon_1 = 650 \pm 280$  or  $300^{+180}_{-150}$ ,  $\epsilon_3 = 4.4^{+1.6}_{-1.4}$ ). Much of the discrepancy is due to the definition of stellar mass: Sullivan et al. and Mannucci et al. apply a correction for dead stars, decreasing stellar mass and correspondingly increasing  $\epsilon$ . Dilday et al. (2008), who measured these parameters using SDSS-SN without correcting for dead stars, obtained  $\epsilon_1 = 230^{+85}_{-78}$  and  $\epsilon_3 = 2.8 \pm 1.2$ . In addition, the values of  $\epsilon_i$  depend on the authors' choice of stellar models and proxies for recent star formation, and may therefore be expected to disagree. Further, while our relative rates for progenitors of different ages are extremely robust to the details of the detection function (Equation 8), the normalization of our rates is less so. A poor estimate of the detection function would multiply all of the rates  $\epsilon_{h,i}$  and  $\epsilon_{l,i}$  in Table 3 by a constant of order unity.

## 6. DISCUSSION AND CONCLUSIONS

### 6.1. Robustness and Systematics

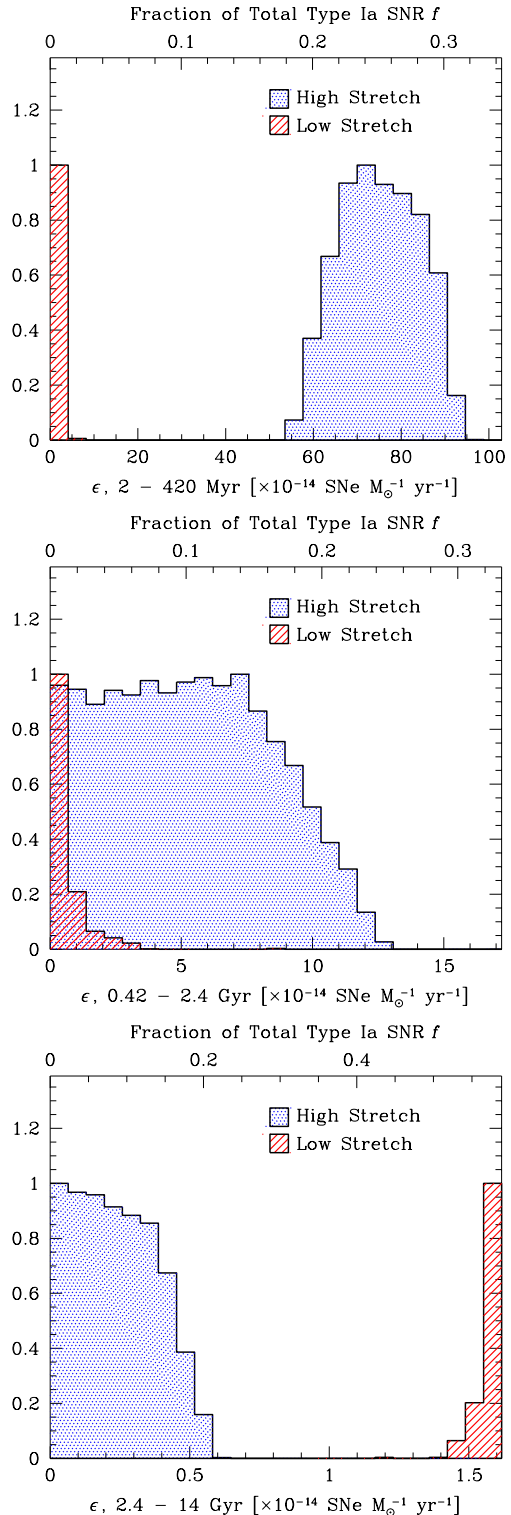


FIG. 7.— The posterior probability distributions of the DTD. The lower horizontal axes give the explosion efficiencies  $\epsilon_{h,i}$  and  $\epsilon_{l,i}$ , the supernova rates per unit stellar mass per year for progenitors in age bin  $i$  (Equation 5). The upper axes show  $f_{h,i}$  and  $f_{l,i}$ , the proportions of the current observed SN Ia rate in the SDSS Stripe 82 galaxies (Equation 10). Nearly all high stretch SNe have progenitors  $\lesssim 400$  Myr old (top panel), while Figure 3 suggests that the typical age may be even younger. Low stretch SNe have a characteristic delay time of at least 2-3 Gyr (bottom panel), with essentially no contribution from young progenitors.

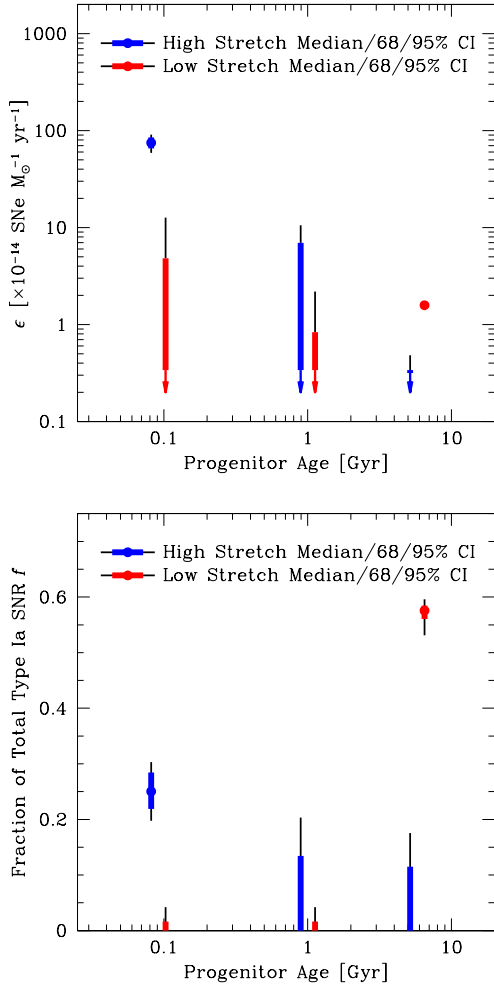


FIG. 8.— The recovered DTDs, expressed in physical units (Equation 5, top panel) and as a proportion of the total SN Ia rate (Equation 10, bottom panel) in the SDSS spectroscopic sample. Upper limits are shown for distributions peaking near zero, medians and two-sided confidence intervals are shown otherwise. Points are drawn at the midpoint of their relevant age ranges (see Table 1), and the high and low stretch bars are offset for ease of viewing.

SDSS-SN is a large, controlled, untargeted survey, and is therefore largely free of systematics in target selection. The subset with host galaxy spectra does have additional selection criteria that can lead to systematics; however, the host galaxies were selected from the entire Stripe 82 spectroscopic sample only through the occurrence of a detectable SN Ia. Further, our comparison of Monte Carlo and observed host galaxies is based not on derived quantities (like stellar masses), but rather on the spectra themselves. We therefore believe our results to be robust. Here, we address several possible sources of bias and argue that all should be minor.

One possible source of systematics is VESPA and its input stellar models (see §3.1). We have chosen our models and the resolution of our recovered star formation histories to minimize these effects. More importantly, we have avoided any use of VESPA on the actual hosts (other than in Figure 2, which we use solely to set the stage), and only use it to select our samples of mock hosts. Therefore, the star formation histories from VESPA will

only bias our results if they are incorrect in the *mean*. The clear evidence of young stars in Figure 3 qualitatively supports the results in Figure 7.

Our earlier paper, Aubourg et al. (2008), used VESPA to show the existence of a prompt component associated with the age bin to 180 Myr. Aubourg et al. and the present manuscript use different approaches to recover information about SN Ia progenitors. While in this paper we aim at recovering the full DTD in the least parametric possible way allowed by the data, in Aubourg et al. we focused on recovering the shortest age of the prompt progenitor channel. It is possible that very young star formation can mask the presence of older stars. This in itself does not remove the requirement for the presence of a young population, as implied by the analysis of Aubourg et al., but in order to avoid this issue, we have taken a cautious approach and combined the young bins into a broad bin. However, the difference spectrum in Figure 3 suggests that the youngest bin in our study may be dominated by progenitors substantially younger than 400 Myr, which would give support to the Aubourg et al. findings. Note that we cannot with these data exclude the possibility that the progenitors are older, as we have demonstrated only that very recent star formation is required to be present. An older progenitor population could be reconciled provided correlations in the star formation rate mean that older star formation is, in the majority of cases, accompanied by a very young population. We are limited by the signal-to-noise ratio of the difference spectrum; with a larger supernova host sample, we should be able to model better the age of the stellar populations of the difference spectrum.

Systematic errors in the shape of the observed spectra will give errors in the VESPA-derived star formation histories. In a sample of physically identical galaxies, such an effect could, for example, produce a subsample with bluer measured spectra and thus younger inferred stellar populations. Selecting galaxies based on their derived masses of young stars will therefore produce average spectra that are too blue. In this way, differences in the average spectra of mock hosts selected by Equation (7) will be exaggerated by using the VESPA-derived masses rather than the (unknown) physical masses. However, this effect would make it *easier* to reproduce the differences in average spectra seen in Figure 3, biasing us *against* the different progenitor ages for high and low stretch SNe Ia seen in Figures 7 and 8. These effects are also small: Adelman-McCarthy et al. (2008) show that spectrophotometric calibrations are accurate to about 4% rms (see their Figures 4 and 5).

Another possible source of systematics is the variation in SN and host galaxy properties. Galaxies with young stellar populations tend to have more dust, which could render SNe associated with younger stellar populations fainter. We have not taken host galaxy dust into account other than by adding scatter to our selection function, through the  $a$  parameter in Equation (8). However, the colors of SNe are measurable and depend in part on host galaxy extinction. As shown in Figure 5, the color parameter recovered by SALT II is uncorrelated with the stretch. Perhaps more surprisingly, it is also uncorrelated with the mean interstellar dust extinction as fit by VESPA. Any systematic variations of color with host galaxy properties must therefore be small, and should

have little effect on our results.

Kelly et al. (2009) have found a hint of another systematic effect, a correlation between peak SN Ia luminosity and host galaxy mass not captured by the color or stretch variation. However, the magnitude of this effect is too small ( $\lesssim 0.1$  magnitude) to significantly impact our study.

In addition to these systematics, we could suffer biases either from our light curve ratings (§3.2) or from our choice of parameters in Equations (8) and (9). To eliminate the former, we did all of the light curve fits and ratings blindly (§3.2), with no knowledge of the host galaxies. For the latter, we took all free parameters in Equation (9) from Guy et al. (2005) and fit the parameters  $m_{lim}$  and  $a$  in our detection efficiency (Equation 8) to match the observed redshift distributions of both high and low stretch SNe. Changing  $m_{lim}$  and  $a$  could multiply all of the recovered explosion efficiencies  $\epsilon$  by a constant of order unity, but our results are otherwise insensitive to the details of the selection function.

Finally, we measure the SN Ia rates in the SDSS spectroscopic sample, which contains fewer low-mass, metal-poor galaxies than a volume-limited sample would. Should SN Ia production be suppressed in low metallicity environments as Kobayashi et al. (1998) and others have suggested, SN Ia rates could be lower in a volume-limited sample than our results would indicate.

### 6.2. Connection to Progenitor Models

It is remarkable how cleanly our observational cut in stretch divides the sample into groups with distinct progenitors. The choice of 0.92 as a division is somewhat arbitrary; it was a guess motivated by Figure 2 and Sullivan et al. (2006). The observed distribution of stretches does not show a clear bimodality (see Figure 5) and indeed appears continuous. It is of course possible that SNe Ia have *more* than two progenitor channels, each distinguished by a range of stretches. However, Figure 2 provides little guidance on where to split either the high or low stretch sample, and in any case, our sample sizes of 60 high stretch and 41 low stretch SNe are too small to profitably subdivide further.

Given the division by stretch into two samples, we can test the compatibility of our DTD with predictions of various progenitor models. We find that many can explain the prompt channel but have extreme difficulty reproducing our low stretch DTD, in which nearly all systems take more than  $\sim 2.4$  Gyr to explode. The theoretical single degenerate DTD calculated by Wang et al. (2010) is compatible with our high stretch sample but falls short of our low stretch rates by at least an order of magnitude (see their Figures 8 and 9). All of the DTDs published by Greggio (2005) have too high a rate from young stars to match our low stretch sample, though several are compatible with our high stretch rates. Ruiter et al. (2009) calculate two-peaked theoretical DTDs for various common envelope scenarios, but with the exception of one semidetached double white dwarf binary model, find rates in young stars inconsistent with our low stretch constraints. It is possible that a single progenitor channel could produce luminous, high stretch objects with a short delay time and subluminal, low stretch objects with a long delay time, perhaps because of different compositions at white dwarf birth. Though recent progress

has been made (Woosley et al. 2007), we still lack an understanding of the dependence of SN Ia stretch on the progenitor composition, and do not attempt to address the likelihood of this scenario in this paper.

### 6.3. Conclusions

We have used SDSS-SN, the only large untargeted supernova survey at low redshift, to constrain the progenitor populations of Type Ia supernovae. The blind nature of the survey renders it free of most systematics, while our use of spectra of both hosts and a large control sample has allowed us to minimize the impact of stellar population models on our results. We dramatically confirm the two populations seen by Sullivan et al. (2006), Mannucci et al. (2006), Scannapieco & Bildsten (2005), Aubourg et al. (2008) and others, finding a “prompt” component of luminous, high stretch SNe with a characteristic delay time  $\lesssim 400$  Myr (the difference spectrum in Figure 3 hints at a time as short as tens of Myr) and a “delayed” component of subluminal, low stretch SNe with a delay time  $\gtrsim 2.4$  Gyr. While our results are in broad agreement with the  $A + B$  model (Equation 1), they place strong constraints on the progenitor ages and cause difficulties for many extant theoretical delay time distributions. We caution against any physical interpretation of the precise values of the age boundaries, which serve only as limits of integration.

Type Ia supernovae have played a key role in our current understanding of the cosmological model. In spite of our incomplete understanding of Type Ia progenitors and explosions, SN Ia surveys like SNLS (Astier et al. 2006), ESSENCE (Wood-Vasey et al. 2007) and SDSS-SN (Kessler et al. 2009) continue to provide the best constraints on cosmological parameters. Further improvements, for example with the JDEM candidate SuperNova Acceleration Probe (SNAP Collaboration: G. Aldering et al. 2004), will require systematic effects in SN Ia standardization to be controlled to 1 – 2%. The identification of the stellar evolution paths that can yield SNe Ia is therefore a key issue: the brightness of a supernova could depend on the nature of its progenitor, and the demographics of SNe Ia would depend on redshift through the evolution time. This could yield an effective, non-cosmological, dependence of the mean “standardized” absolute magnitude on redshift that would bias dark energy measurements. In principle such an effect could be advantageous, as analyses of host spectra could be used to determine the probabilities of each progenitor route, and hence the use of the appropriate Phillips (1993) stretch-luminosity relation. This will require both better constraints on Type Ia progenitor models and an improved understanding of the Phillips relation.

While Type Ia supernovae are most widely studied because of their use as standard candles, they are also dynamically important in the interstellar medium and are believed to be the main source of iron-peak elements. A fast route to Type Ia supernovae therefore has implications for the interpretation of alpha-enhancement. If most SNe Ia are old, iron enrichment will be significantly delayed from the onset of star formation, and alpha-enhancement will be associated with short-lived periods of relatively recent star formation. Significant early iron production by “prompt” SNe Ia would mod-

ify this conclusion, making it more difficult to explain alpha-enhancement and supporting alternative explanations such as a modification of the initial mass function.

Future studies will certainly improve on our results; the Baryon Oscillation Spectroscopic Survey (BOSS, Schlegel et al. 2007), part of SDSS-III<sup>8</sup>, is perhaps the most promising. BOSS is taking spectra of all supernova hosts from SDSS-SN, expanding our sample by a factor of  $\sim 3$ . While a control sample is not naturally defined for these SN hosts, the untargted nature of SDSS-SN means that a control group could be built out of a deep, volume-limited sample of galaxies like GAMA (Baldry et al. 2009). Such a sample could be used to significantly tighten our error bars.

Increasing the temporal resolution of our recovered DTD may be more challenging. This will require better spectra, both of SN hosts and control galaxies, and especially better stellar population synthesis models. The latter point is crucial: we had to combine all ages younger than 420 Myr into a single bin because of biases introduced by the modeling of dust and stellar spectra. Splitting this age bin will allow us to better determine the timescale of “prompt” SNe Ia and thus the initial masses of their progenitors.

With better stellar population synthesis models, BOSS, GAMA, and other surveys would hold tremendous promise. They would allow us to construct a sample several times as large as the one used here, and with better recovered star formation histories. With such a sample, we could improve both the precision and temporal resolution of our DTD by a factor of  $\sim 2$ , placing strict constraints on theoretical SN Ia progenitor models.

## 7. ACKNOWLEDGMENTS

Funding for the SDSS and SDSS-II has been provided by the Alfred P. Sloan Foundation, the Partic-

ipating Institutions, the National Science Foundation, the U.S. Department of Energy, the National Aeronautics and Space Administration, the Japanese Monbukagakusho, the Max Planck Society, and the Higher Education Funding Council for England. The SDSS Web Site is <http://www.sdss.org/>.

The SDSS is managed by the Astrophysical Research Consortium for the Participating Institutions. The Participating Institutions are the American Museum of Natural History, Astrophysical Institute Potsdam, University of Basel, University of Cambridge, Case Western Reserve University, University of Chicago, Drexel University, Fermilab, the Institute for Advanced Study, the Japan Participation Group, Johns Hopkins University, the Joint Institute for Nuclear Astrophysics, the Kavli Institute for Particle Astrophysics and Cosmology, the Korean Scientist Group, the Chinese Academy of Sciences (LAMOST), Los Alamos National Laboratory, the Max-Planck-Institute for Astronomy (MPIA), the Max-Planck-Institute for Astrophysics (MPA), New Mexico State University, Ohio State University, University of Pittsburgh, University of Portsmouth, Princeton University, the United States Naval Observatory, and the University of Washington.

We thank an anonymous referee for many corrections and helpful suggestions. We would also like to thank the entire SDSS collaboration and especially the SDSS Supernova Survey team for their work in building the exceptional dataset used in this paper.

This material is based upon work supported under a National Science Foundation Graduate Research Fellowship to TDB. It was also supported in part by DOE grant DE-FG02-07ER41514. RT thanks the UK Science and Technology Facilities Council and the Leverhulme Trust for financial support.

<sup>8</sup> <http://www.sdss3.org/cosmology.php>

## REFERENCES

- Abazajian, K. N., et al. 2009, *ApJS*, 182, 543  
 Adelman-McCarthy, J. K., et al. 2008, *ApJS*, 175, 297  
 Adelman-McCarthy, J. K., et al. 2006, *ApJS*, 162, 38  
 Astier, P., et al. 2006, *A&A*, 447, 31  
 Aubourg, É., Tojeiro, R., Jimenez, R., Heavens, A., Strauss, M. A., & Spergel, D. N. 2008, *A&A*, 492, 631  
 Badenes, C., Harris, J., Zaritsky, D., & Prieto, J. L. 2009, *ApJ*, 700, 727  
 Baldry, I. K., et al. 2009, [arXiv:0910.5120](http://arxiv.org/abs/0910.5120)  
 Cooper, M. C., Newman, J. A., & Yan, R. 2009, *ApJ*, 704, 687  
 Dilday, B., et al. 2008, *ApJ*, 682, 262  
 Eisenstein, D. J., et al. 2001, *AJ*, 122, 2267  
 Fitzpatrick, E. L. 1999, *PASP*, 111, 63  
 Frieman, J. A., et al. 2008, *AJ*, 135, 338  
 Furusawa, H., et al. 2008, *ApJS*, 176, 1  
 Gal-Yam, A., & Maoz, D. 2004, *MNRAS*, 347, 942  
 Gallagher, J. S., Garnavich, P. M., Berlind, P., Challis, P., Jha, S., & Kirshner, R. P. 2005, *ApJ*, 634, 210  
 Greggio, L. 2005, *A&A*, 441, 1055  
 Gunn, J. E., et al. 1998, *AJ*, 116, 3040  
 Gunn, J. E., et al. 2006, *AJ*, 131, 2332  
 Guy, J., et al. 2007, *A&A*, 466, 11  
 Guy, J., Astier, P., Nobili, S., Regnault, N., & Pain, R. 2005, *A&A*, 443, 781  
 Hamuy, M., Phillips, M. M., Suntzeff, N. B., Schommer, R. A., Maza, J., Smith, R. C., Lira, P., & Aviles, R. 1996, *AJ*, 112, 2438  
 Hicken, M., Wood-Vasey, W. M., Blondin, S., Challis, P., Jha, S., Kelly, P. L., Rest, A., & Kirshner, R. P. 2009, *ApJ*, 700, 1097  
 Holtzman, J. A., et al. 2008, *AJ*, 136, 2306  
 Howell, D. A. 2001, *ApJ*, 554, L193  
 Kelly, P. L., Hicken, M., Burke, D. L., Mandel, K. S., & Kirshner, R. P. 2009, [arXiv:0912.0929](http://arxiv.org/abs/0912.0929)  
 Kessler, R., et al. 2009, *ApJS*, 185, 32  
 Kobayashi, C., Tsujimoto, T., Nomoto, K., Hachisu, I., & Kato, M. 1998, *ApJ*, 503, L155  
 Laplace, P. 1814, *Essai Philosophique sur les Probabilités* (New York: Dover)  
 Mannucci, F., Della Valle, M., & Panagia, N. 2006, *MNRAS*, 370, 773  
 Mannucci, F., Della Valle, M., Panagia, N., Cappellaro, E., Cresci, G., Maiolino, R., Petrosian, A., & Turatto, M. 2005, *A&A*, 433, 807  
 Maoz, D., Mannucci, F., Li, W., Filippenko, A. V., Della Valle, M., & Panagia, N. 2010, [arXiv:1002.3056](http://arxiv.org/abs/1002.3056)  
 Maraston, C. 2005, *MNRAS*, 362, 799  
 Neill, J. D., et al. 2006, *AJ*, 132, 1126  
 Neill, J. D., et al. 2009, *ApJ*, 707, 1449  
 Nugent, P., Kim, A., & Perlmutter, S. 2002, *PASP*, 114, 803  
 Perlmutter, S., et al. 1999, *ApJ*, 517, 565  
 Petrosian, V. 1976, *ApJ*, 209, L1  
 Phillips, M. M. 1993, *ApJ*, 413, L105  
 Pritchett, C. J., Howell, D. A., & Sullivan, M. 2008, *ApJ*, 683, L25  
 Riess, A. G., et al. 1998, *AJ*, 116, 1009  
 Ruiter, A. J., Belczynski, K., & Fryer, C. 2009, *ApJ*, 699, 2026

- Sako, M., et al. 2008, *AJ*, 135, 348
- Scannapieco, E., & Bildsten, L. 2005, *ApJ*, 629, L85
- Schawinski, K. 2009, *MNRAS*, 397, 717
- Schlegel, D. J., et al. 2007, in *Bulletin of the American Astronomical Society*, Vol. 38, *Bulletin of the American Astronomical Society*, 966
- Schlegel, D. J., Finkbeiner, D. P., & Davis, M. 1998, *ApJ*, 500, 525
- Silva, D. R., & Cornell, M. E. 1992, *ApJS*, 81, 865
- SNAP Collaboration: G. Aldering, et al. 2004, [arXiv:astro-ph/0405232](https://arxiv.org/abs/astro-ph/0405232)
- Strauss, M. A., et al. 2002, *AJ*, 124, 1810
- Sullivan, M., et al. 2010, [arXiv:1003.5119](https://arxiv.org/abs/1003.5119)
- Sullivan, M., et al. 2006, *ApJ*, 648, 868
- Tojeiro, R., Heavens, A. F., Jimenez, R., & Panter, B. 2007, *MNRAS*, 381, 1252
- Tojeiro, R., Wilkins, S., Heavens, A. F., Panter, B., & Jimenez, R. 2009, *ApJS*, 185, 1
- Totani, T., Morokuma, T., Oda, T., Doi, M., & Yasuda, N. 2008, *PASJ*, 60, 1327
- van den Bergh, S., Li, W., & Filippenko, A. V. 2005, *PASP*, 117, 773
- Wang, B., Li, X., & Han, Z. 2010, *MNRAS*, 401, 2729
- Wood-Vasey, W. M., et al. 2007, *ApJ*, 666, 694
- Woosley, S. E., Kasen, D., Blinnikov, S., & Sorokina, E. 2007, *ApJ*, 662, 487
- York, D. G., et al. 2000, *AJ*, 120, 1579